Gas-phase isopropanol degradation by nonthermal plasma combined with Mn-Cu/-Al$_2$O$_3$

Ken-Lin Chang[1,2] • Yu-Chieh Lin[1] • Ming-Ze Qiu[1] • Chun-Wei Tu[3] • Chih-Ping Chang[3] • Jhong-Lin Wu[3] •
Yung-Chang Lin[4,5,6] • Chien-Kuei Chang[7]

Abstract

In this study, the dielectric barrier discharge (DBD) induced by nonthermal plasma (NTP) technology was used for isopropanol (IPA) degradation. IPA, intermediate, final product, and ozone concentrations were analyzed using GC-MS, carbon dioxide detector, and ozone detector. The experimental flow rate and concentration were fixed to 1 L/min and 1200 ppm ± 10%, respectively. Different reaction procedures were proposed for self-made metal catalyst combined with a plasma system (plasma alone and γ-Al$_2$O$_3$ combined with plasma, Cu (5 wt%)/γ-Al$_2$O$_3$ combined with plasma, Mn (3 wt%)-Cu (5 wt%)/γ-Al$_2$O$_3$ combined with plasma). In addition, the effect of the carrier gas oxygen content (0%, 20%, and 100%) on IPA conversion and intermediate and carbon dioxide selectivity was also investigated. The results revealed that the Mn (F)-Cu/γ-Al$_2$O$_3$ combined with plasma exhibited more efficient IPA conversion. In the 100% oxygen environment, the IPA conversion rate increased from 79.32 to 99.99%, and carbon dioxide selectivity increased from 3.82 to 50.23%. IPA was completely converted after 60 min of plasma treatment with the acetone selectivity, carbon dioxide selectivity, and tail ozone concentration of 26.71% ± 1.27%, 50.23% ± 0.56%, and 1761 ± 11 ppm, respectively. This study proved that the current single planar DBD configuration is an effective advanced treatment technology for the decomposition of VOCs.

Keywords Volatile organic compound · Dielectric barrier discharge · Isopropyl alcohol · Metal catalyst

Responsible Editor: Vítor Pais Vilar

✉ Chien-Kuei Chang
isaac@nkust.edu.tw

[1] Institute of Environmental Engineering, National Sun Yat-Sen University, Kaohsiung, Taiwan

[2] Department of Public Health, College of Health Sciences, Kaohsiung Medical University, Kaohsiung, Taiwan

[3] Environmental Resource and Management Research Center, National Cheng Kung University, Tainan, Taiwan

[4] Department of Electrical Engineering, Cheng Shiu University, Kaohsiung, Taiwan

[5] Department of Electrical Engineering, Cheng Shiu University, Kaohsiung, Taiwan

[6] Center for environmental Toxin and Emerging Contaminant Research, Cheng Shiu University, Kaohsiung, Taiwan

[7] Department of Chemical and Materials Engineering, National Kaohsiung University of Science and Technology, Kaohsiung, Taiwan

Introduction

In Taiwan, the high-tech industry, including photovoltaic and semiconductor industries, is a leading industry; its development is actively supported by Taiwan government. In the photovoltaic and semiconductor industries, during the manufacturing processes, organic solvents are often added for cleaning; this leads to volatile organic compound (VOC) formation and other environmental problems. Of the VOCs formed, isopropanol (IPA) is a main pollutant (Debono et al. 2018). Therefore, research on fast, effective, and economical IPA processing technology is crucial to resolving the aforementioned environmental problems.

Traditional VOC control technologies include condensation (Belaissaoui et al. 2016), adsorption (Ohshima et al. 2010), catalyst incineration (Yang et al. 2019), and biological treatment (Mohamed et al. 2016). However, these technologies have their own disadvantages such as large energy consumption for condensation, adsorption, and incineration (Vandenbroucke et al. 2011); limited concentration ranges

for condensation and biological treatment (Khan and Kr Ghoshal 2000); and slow removal rates for biological treatment. Therefore, novel control technologies, such as plasma destruction, are researched and applied in industries. Plasma is divided into high- and low-temperature systems, and low-temperature plasma systems include glow discharge (Fandino et al. 2018), corona discharge (Malik et al. 2005; Rodrigo et al. 2005), and DBD (Li et al. 2020). DBD exhibit an advantage of rapidly destroying gaseous pollutants under normal temperature and pressure (Li et al. 2020). The underlying principle is to place a dielectric material such as quartz on a high-voltage electric board. When a high alternating current is applied to a high-voltage electric board, a carrier gas in a discharge gap space is ionized to form strong oxidants such as free radicals and ozone to oxidize VOCs.

Regarding ozone generated using the low-temperature plasma system, Dhandapani and Oyama (1997) reported that p-type oxides demonstrate a high activity for decomposing ozone, and MnO_2 exhibits the most favorable decomposing ozone activity and can decompose ozone into O_2^- or O_2^{2-} by using a catalyst, which has a positive effect on VOC decomposition in low-temperature plasma systems. Li et al. (1998) used a Raman spectrometer to study ozone decomposition by using a manganese oxide–loaded catalyst and found that when ozone was close to the manganese oxide catalyst surface, it is decomposed into oxygen atoms and atomic oxygen species, and the produced oxygen atoms covered the catalyst surface. Oxygen atoms covering surface reacted with ozone molecules to form peroxide intermediates and gas-phase oxygen molecules. Finally, peroxide intermediates decomposed and desorbed themselves onto oxygen molecules. Therefore, IPA was catalytically oxidized using low-temperature plasma systems. Moreover, many studies have used manganese oxides as active metals. Oxygen atoms or peroxides decomposed because the aforementioned reasons can effectively decompose with IPA to produce other intermediates or final products (Karuppiah et al., 2010; Sivachandiran et al. 2015). Shiau et al. (2017) showed that part of IPA is converted into acetone and CO_2 during NTP desorption process. Sivachandiran et al. (2014) reported that acetone is the most stable intermediate during the oxidation of IPA and requires more energy to decompose. Moreover, copper oxide has high acetone removal efficiency. Zhu et al. (2015) reported that the main reason is the strong surface oxygen activity of the catalyst, which can be achieved using CuO_X, making its reducibility stronger than that of other metal oxide catalysts.

According to the aforementioned literatures, manganese oxidizes IPA by using atomic oxygen generated through ozone decomposition, and copper exhibits a suitable degradation effect on acetone. Spasova et al. (2007) studied the low-temperature ozone decomposition of copper-manganese oxide supported on γ-Al_2O_3. The active phase

on a Cu-Mn/γ-Al_2O_3 catalyst typically comprises Cu^{2+} and Mn^{3+}, increasing the effectiveness of ozone decomposition. Therefore, Cu/Mn catalyst was used in this study. The loading order of copper and manganese is also crucial. Loading order produces different results for VOC decomposition (Qin et al. 2016). In this study, a manganese-copper oxide–mixed catalyst was prepared, and a Cu/Mn oxide catalyst loading sequence was changed to obtain a different catalyst for IPA conversion. The high oxygen content of the carrier gas increases the conversion rate (Kim et al. 2008); thus, we also compared the oxygen content of the carrier gas (0%, 20%, and 100%).

Experimental

Catalyst preparation

Here, the metal catalyst production was based on incipient wetness impregnation (Sudhakaran et al. 2017). Consider Mn (3 wt%)–Cu (5 wt%)/γ-Al_2O_3 an example. First, the estimated water absorption of activated alumina (Eikme International Ltd., Hsinchu, Taiwan) was 0.54 mL/g, which was then ground through 12- and 20-mesh sieves. The activated alumina ground using the 20-mesh sieve was used. A required amount of deionized water was added to an electromagnetic mixer (C-MAG HS7, IKA, Germany) with 1.45 and 2.03 g of manganese nitrate tetrahydrate (98%, Alfa Aesar, MA, USA) and cupric nitrate (99%, Showa Chemicals, Japan), respectively. The resulting solution was stirred at 25 °C and 250 rpm to completely dissolve the solid in deionized water and then was poured into a crucible filled with 10 g of activated alumina, which was placed in an oven (RHD45, Prema, Taiwan) to dry at 105 °C for 1 day. The crucible was placed in a tube-type high-temperature forging furnace and calcined at 500 °C for 5 h in the atmosphere to prepare a catalyst with the metal loading of Mn (3 wt%)–Cu (5 wt%)/
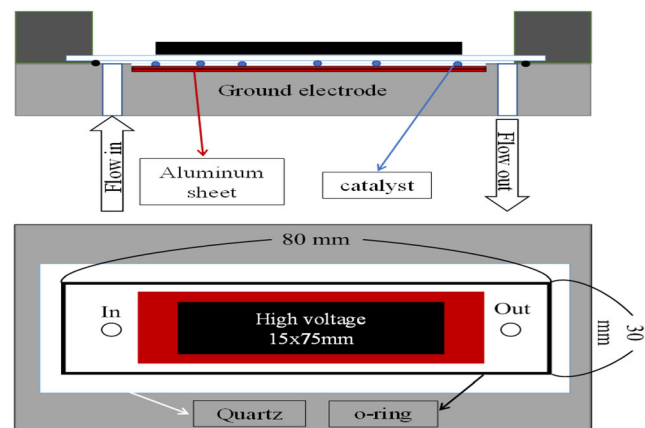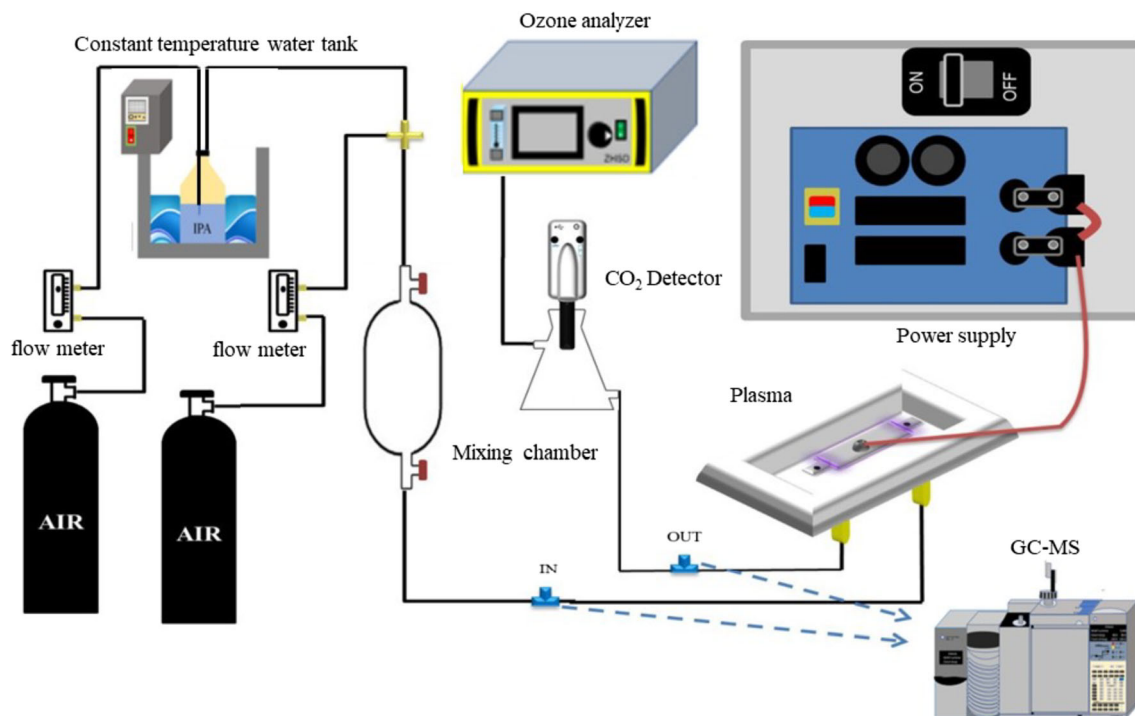

Fig. 1 Concept of DBD discharge reactor

Fig. 2 The schematic diagram of experimental setup

γ-Al$_2$O$_3$. To prepare the catalyst with different loading sequences of metal, first, 1.45 g of manganese nitrate tetrahydrate was added to the required amount of deionized water, and the resulting solution was stirred at 25 °C and 250 rpm with a magnetic stone mixer to completely dissolve the solid in deionized water and then poured into full load. In the oven, 10 g of activated alumina was placed at 105 °C for 1 day for drying. Activated alumina was placed in a tube-type high-temperature calciner activated in air at 500 °C for 5 h for calcination. After activated alumina was cooled to room temperature, the required amount of deionized water was added in 2.03 g of copper nitrate trihydrate. Calcination was repeated under the same aforementioned conditions to prepare Mn (F) (3 wt%)–Cu (5 wt%)/γ-Al$_2$O$_3$ catalyst. Mn (3 wt%)–Cu (F) (5 wt%)/γ-Al$_2$O$_3$ was prepared by adding a metal salt by following the aforementioned procedure, and 1 g of the catalyst was placed in a dielectric barrier discharge (DBD) reactor. Metal weight (wt%) was calculated as follows (Huang et al. 2008):

$$\text{Metal weight (wt\%)} = \frac{\text{W (Metal)}}{\text{W (Carrier)} + \text{W (Metal)}} \times 100\%$$

where W (metal) is the metal weight (in g) and W (carrier) is the carrier weight (in g).

Reactor and plasma parameters

The IPA (99%, J.T.Baker® Chemicals, USA) gas was produced through aeration (Li et al. 2014; Tang et al. 2013). The cylinders of two bottles of synthetic air were divided into two

pipelines. One pipeline used needle valve to control the cylinder pressure and enter the aeration bottle placed in a water tank with constant temperature. IPA was volatilized, and its flow rate controlled using a flow meter was 0.03 L/min. In the other pipeline, the flow rate was 0.97 L/min. After volatilized IPA entered a 1-L mixing bottle, its concentration was adjusted at 1200 ppm ± 10%. Experiment was performed at a total flow rate of 1 L/min. The gas flow temperature was controlled at 26 °C and dry air, and a three-way valve was used to enter the DBD reactor after the gas flow rate and concentration were stabilized. The effect of a change in oxygen content of the carrier gas on the catalyst-plasma system was analyzed. The cylinder of synthetic air was replaced with different cylinders of nitrogen and oxygen.

In the DBD reactor, a 7.5 × 1.5-cm^2 aluminum sheet and an aluminum plate were used as high-voltage and ground electrodes, respectively. The volume of reaction chamber and gas residence time were 8 × 3 × 0.3 cm^3

Table 1 Code comparison for different reaction procedures

Procedures	Code
Plasma alone	P
γ-Al$_2$O$_3$ combine plasma	P + γ
Cu/γ-Al$_2$O$_3$ combine plasma	P + Cu
Mn - Cu/γ-Al$_2$O$_3$ combine plasma	P + Mn – Cu
Mn – Cu (First)/γ-Al$_2$O$_3$ combine plasma	P + Mn – Cu (F)
Mn (First) - Cu/γ-Al$_2$O$_3$ combine plasma	P + Mn (F) – Cu

Table 2 Results of quantitative ICP-AES analysis of each catalyst

	γ-Al$_2$O$_3$	Cu/γ-Al$_2$O$_3$	Mn - Cu/γ-Al$_2$O$_3$	Mn - Cu(F)/γ-Al$_2$O$_3$	Mn(F) - Cu/γ-Al$_2$O$_3$
Cu (wt%)	N.D.	4.89 ± 0.11	4.28 ± 0.04	4.37 ± 0.02	4.83 ± 0.10
Mn (wt%)	N.D.	N.D.	1.92 ± 0.04	1.97 ± 0.01	2.17 ± 0.07

and 0.43 s, respectively. The total power of the system was measured using a plug-in power monitor (AXE-1; AXE Technology Corp., Taiwan) with 24.5 W, and the discharge frequency was measured using an oscilloscope (MDO 704; PINTECH, Guangzhou, China) with 6.1 kHz, a high-voltage probe (HVP-39pro, Pintek,. New Taipei, Taiwan), and average AC discharge voltage of 9.7 kV. The quartz plate was used as dielectric material. Figures 1 and 2 illustrate the DBD reactor concept and experimental setup, respectively.

Catalyst characterization

The catalyst was characterized and analyzed to determine its various characteristics by using the following analytical equipment: Inductively coupled plasma atomic emission spectroscopy (Optima 2000DV, Perkin Elmer, Shelton, CT, USA) was employed to identify manganese and copper loadings. A scanning electron microscope (FEI Quanta 200, FEI, Netherland) was used to investigate the changes in manganese and copper metal oxides present on the catalyst surface. An X-ray photoelectron spectroscope (Sigma Probe, Thermo VG Scientific, Waltham, MA, USA) was used to identify the electronic valence of manganese and copper metal oxides on the catalyst surface, and Brunauer-Emmett-Teller (BET) instrument (ASAP 2020 Plus Chemisorption, Micromeritics, USA) was used to determine the specific surface area, porosity, and pore size of activated alumina and the catalyst.

Monitoring instrument, calculation formula, and code

Gas chromatography–mass spectrometry (GC-MS; 7890A - 5975C; Agilent, USA) and column DB-WAX (30 m × 0.25 mm × 0.5 μm; Agilent-J&W, USA) were used to analyze IPA concentrations before and after reactor treatment and acetone concentrations obtained at an outlet. The CO$_2$ concentration was monitored using a CO$_2$ detector (Wireless CO$_2$ Sensor-PS3208, PASCO, USA), and the tail ozone concentration was analyzed using an O$_3$ concentration analyzer (UVOZ-3000 benchtop ozone concentration gas analyzer, Automation Technology, China).

To statistically determine whether a considerable difference exists between various parameters, SPSS (version 24; IBM) was used. To compare the multiple groups of two repeated data, one-way analysis of variance was used to obtain multiple comparisons to explore the differences between multiple data sets and multiple comparisons. Many different methods for multiple comparison are available, among which the least significant difference is the most widely accepted method in studies. The experimental data were tested in duplicate, and an average of the two replicates was used to obtain a standard error. To obtain the IPA conversion rate, acetone selectivity, and carbon dioxide selectivity, the following calculation formulas were used:

$$\text{IPA Conversion Rate}(\%) = \frac{[\text{IPA}]\text{Inlet} - [\text{IPA}]\text{Outlet}}{[\text{IPA}]\text{Inlet}} \times 100\%$$

$$\text{Acetone Selectivity}(\%) = \frac{[\text{Acetone}]}{[\text{IPA}]\text{Inlet} - [\text{IPA}]\text{Outlet}} \times 100\%$$

$$\text{Carbon Dioxide Selectivity}(\%) = \frac{[\text{Carbon Dioxide}]}{3([\text{IPA}]\text{Inlet} - [\text{IPA}]\text{Outlet})} \times 100\%$$

Table 1 presents the different reaction procedures in code form.

Table 3 Specific surface area, pore volume, and pore value of each catalyst

	S_{BET} (m^2/g)	BJH average volume of pore (cm^3/g)	BJH average pore diameter (nm)
γ-Al$_2$O$_3$	275.80	0.50	6.38
Cu/γ-Al$_2$O$_3$	225.55	0.48	6.99
Mn-Cu/γ-Al$_2$O$_3$	220.36	0.45	6.88
Mn-Cu(F)/γ-Al$_2$O$_3$	201.22	0.46	7.51
Mn(F)-Cu/γ-Al$_2$O$_3$	200.08	0.45	7.40

Results and discussion

Catalyst characteristics analysis

Determination of metal content using ICP-AES

Table 2 presents the results of the ICP-AES analysis. For Cu/γ-Al$_2$O$_3$, the same as results of energy-dispersive X-ray spectroscopy, copper exhibited the highest metal content of 4.89 wt% that was closest to the theoretical metal content. In Mn (F)-Cu/γ-Al$_2$O$_3$, manganese exhibited the highest metal content of 2.17 wt% that was closest to the theoretical metal content.

Specific surface area analysis by using BET

Table 3 presents the specific surface area (S$_{BET}$), Barret-Joyner-Halenda (BJH) average volume of pore, and BJH average pore diameter. With the addition of copper and manganese oxide, S$_{BET}$ and BJH average volume of pore gradually decreased. This result is consistent with scanning electron microscopic (SEM) observations. Some metal oxide particles covered the surface of γ-Al$_2$O$_3$ because the pore diameter was larger than the pore size of the carrier (Zhu et al. 2016). The BJH average pore diameter increased with the mental load, which can cause by blocking micropores (Zakaria et al. 2012).

Fig. 3 X-ray photoelectron spectroscopic spectrum of (**a**) Cu2p and (**b**) Mn2p
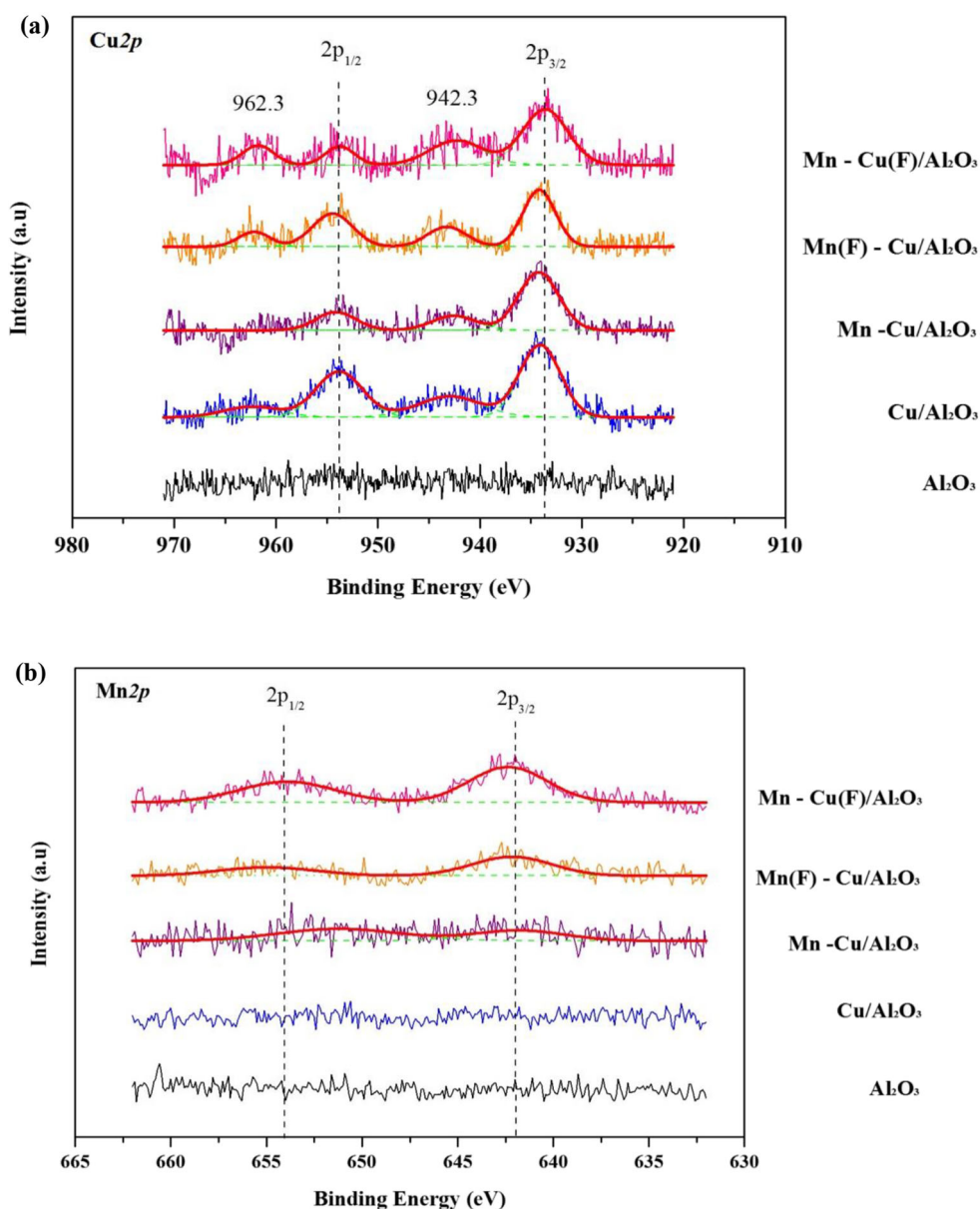
Identification of surface chemical state through X-ray photoelectron spectroscopy

Figure 3 a presents the X-ray photoelectron spectroscopic spectrum of Cu at 2p. Cu exhibits a $2p_{3/2}$ peak at the position of the binding energy of 933.5 eV (Tahir et al. 2018). The spin-orbit splitting indicated a $2p_{1/2}$ peak at 953.8 eV. The two peaks were separated by 20.3 eV, which is consistent with value reported in the literature. Near $2p_{1/2}$, due to the satellite characteristics of Cu^{2+}, strong peaks appeared at 962.3 and 942.3 eV, and no overlapping of other peaks was noted through peak fitting, indicating that the Cu valence state in the catalyst was Cu^{2+}.

Figure 3 b presents the X-ray photoelectron spectroscopic spectrum of Mn at 2p. Mn exhibits a peak of $2p_{3/2}$ at the position of the binding energy of 641.7 eV (Todorova et al. 2010). The spin-orbit splitting indicated a peak of $2p_{1/2}$ at 653.2 eV. The two peaks were 11.5 eV apart, according to the literature. Of them, the peaks of Mn^{3+} and Mn^{4+} exhibited no obvious satellite characteristics, and their binding energies were quite close, which makes it difficult to know the exact. For the electron valence state, although Mn was divided using peak fitting, no overlaps including other peaks were obtained in the fitting results. Therefore, the binding energy of Mn_2O_3 of 641.5–641.7 eV indicated that Mn existed on the catalyst as an electron valence Mn^{3+}.

Fig. 4 SEM images of each catalyst: (i) γ-Al_2O_3, (ii) Cu/γ-Al_2O_3, (iii) Mn-Cu/γ-Al_2O_3, (iv) Mn-Cu (F)/γ-Al_2O_3, and Mn (F)-Cu/γ-Al_2O_3 ($\times$ 20,000 magnification)
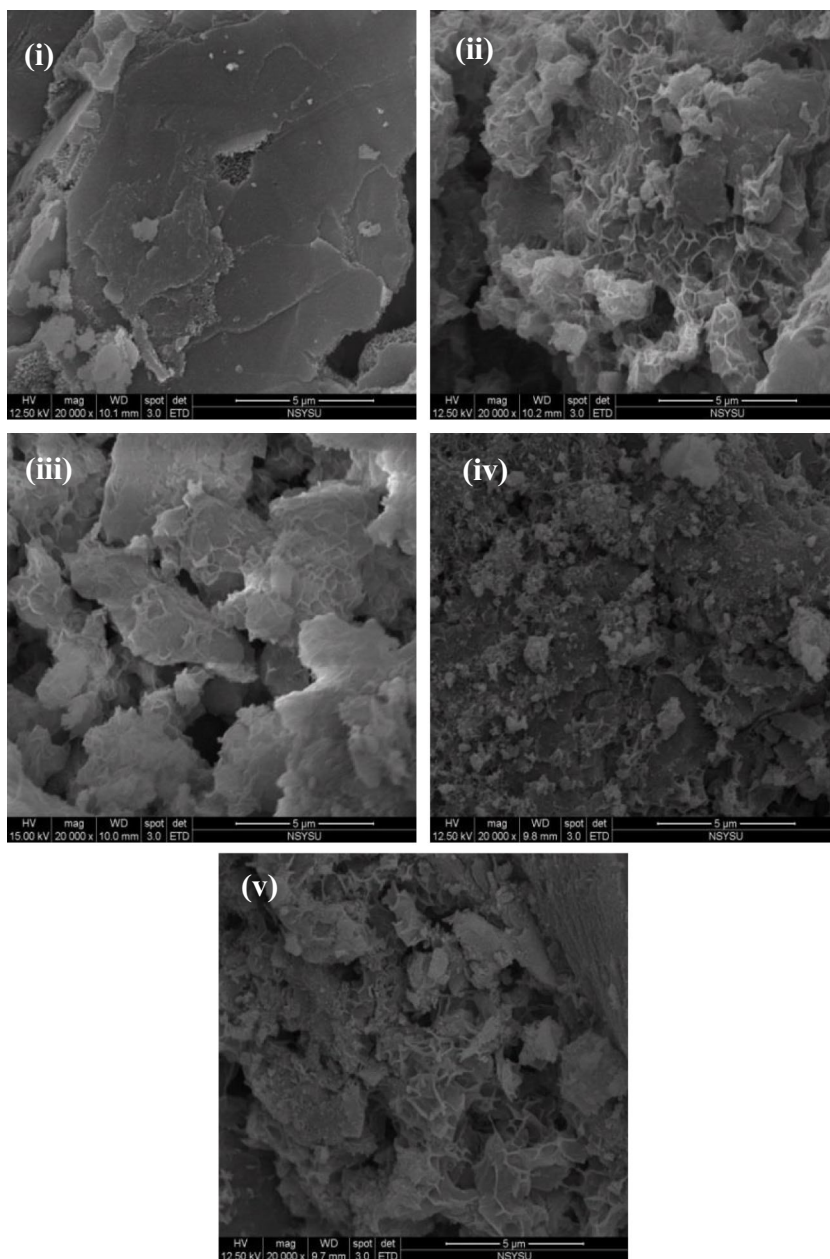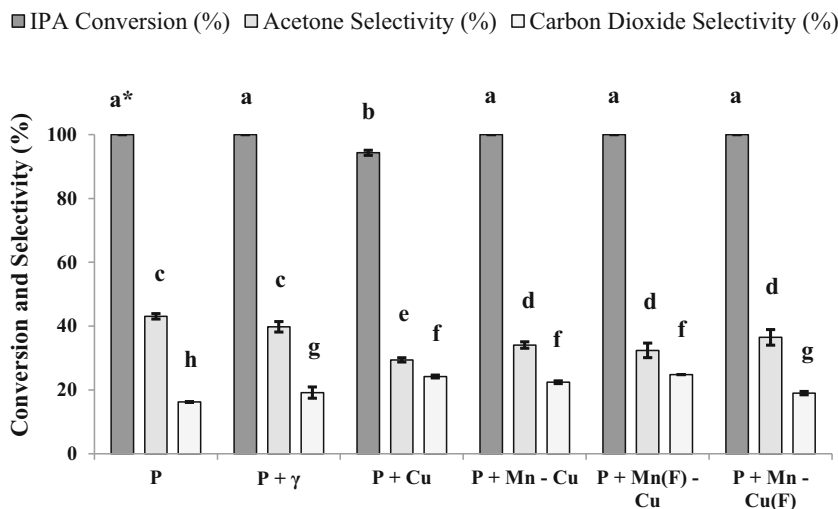
Fig. 5 Comparison between different reaction procedures. The letters presented above represent the significant analysis; the same letters represent nonsignificant difference in the results of pairwise comparisons, and different letters represent significant differences in the results of pairwise comparisons

On the basis of the aforementioned literature and results, the oxidation states of Cu and Mn in the catalyst were CuO and Mn_2O_3. Moreover, this result is consistent with the explanation of Cu and Mn in the electron valence state for ozone decomposition (Spasova et al. 2007).

SEM images

Figure 4 illustrates the surface structure of metal oxide before and after loading, wherein (i), (ii), (iii), (iv), and (v) represent γ-Al_2O_3, Cu/γ-Al_2O_3, Mn-Cu/γ-Al_2O_3, Mn-Cu (F)/γ-Al_2O_3, and Mn (F)-Cu/γ-Al_2O_3 with × 20,000 magnification, respectively. Figure 4 reveals the formation of copper and manganese oxide crystals on each catalyst, and the crystal shape was similar to that reported in the literature (Wang et al. 2017).

Comparison of different reaction procedures

Operating conditions were as follows: airflow temperature 26 °C, dry air, carrier gas with 20% oxygen, 3-mm discharge gap,

and 60-min oxidation time. Figure 5 presents the comparison between different reaction procedures.

P + Cu exhibited considerable differences in both the acetone and carbon dioxide selectivity but provided inadequate results for IPA conversion. Zhu et al. (2015) reported that acetone oxidization was easier on the surface of copper oxide than on that of other metal oxides.

From the S_{BET} results, Cu/γ-Al_2O_3 was assumed to be easier to adsorb, pulverize, and oxidize than were other catalysts when the active sites of copper and manganese oxides were absorbed by γ-Al_2O_3. Compete with ozone to absorb active sites, because active sites that can decompose ozone were reduced. This finding can explain the reason for the lower IPA conversion of P + Cu than that of other reaction procedures. According to the literature, manganese oxide is a p-type oxide and therefore exhibits the effect of decomposing ozone into O_2^- or O_2^{2-} (Dhandapani and Oyama 1997). O_2^- or O_2^{2-} can be used to decompose IPA rapidly. Therefore, P + Mn (F)-Cu was the most effective among the three parameters. The ICP-AES results of Mn (F)-Cu/γ-Al_2O_3 indicated the

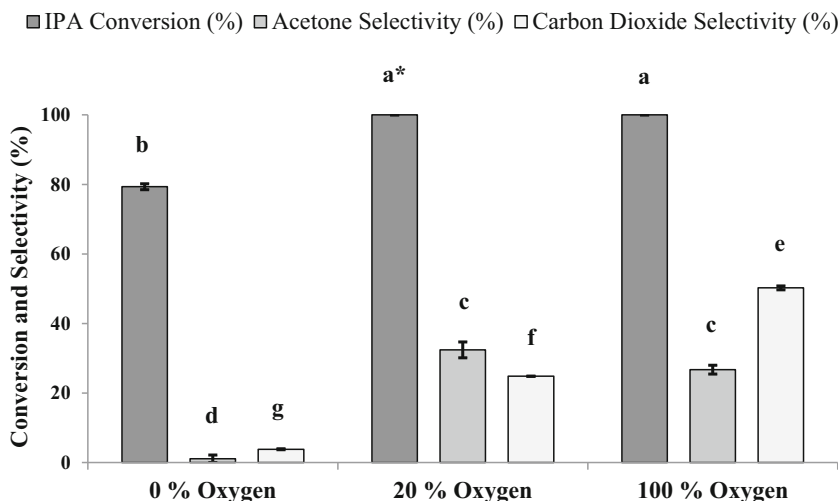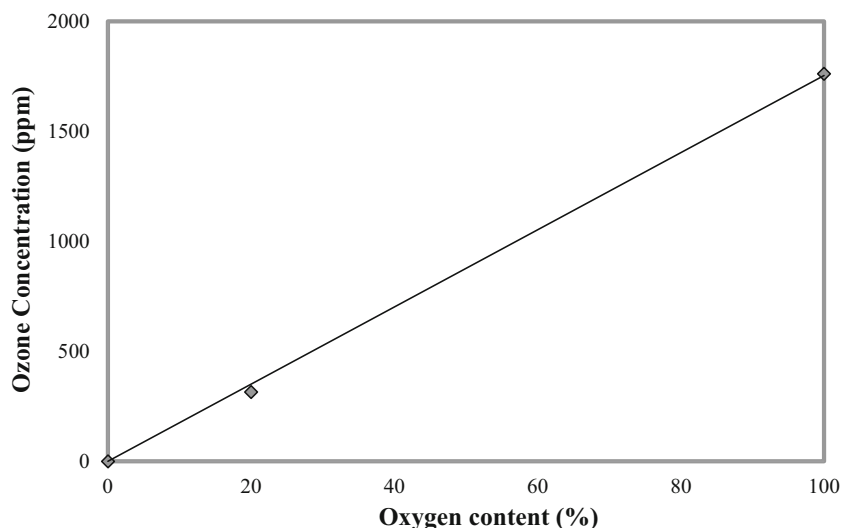**Fig. 6** Comparison of changes in oxygen content of the carrier gas at 60-min reaction

Fig. 7 Ozone concentration for changing oxygen content in carrier gas

highest manganese and copper contents in the loading order. The priority supported manganese can be well dispersed on γ-Al$_2$O$_3$, which causes ozone to effectively react with manganese oxide in the inner layer for decomposing and oxidizing IPA adsorbed during the reaction. Moreover, copper oxide on the outer layer could decompose acetone. On the basis of these results, Mn (F)-Cu /γ-Al$_2$O$_3$ was used as the most suitable catalyst to explore the oxygen content of the carrier gas.

Effect of oxygen content in carrier gas on catalyst and plasma system

Operating conditions were as follows: air temperature, 26 °C; dry air; carrier gas oxygen content, 0%, 20%, and 100%; discharge gap, 3 mm; and oxidation time, 60 min. The most suitable catalyst P + Mn (F)-Cu obtained from the experiment was used to study the oxygen content of the carrier gas. Figure 6 presents the comparison of the oxygen content in different carrier gases.
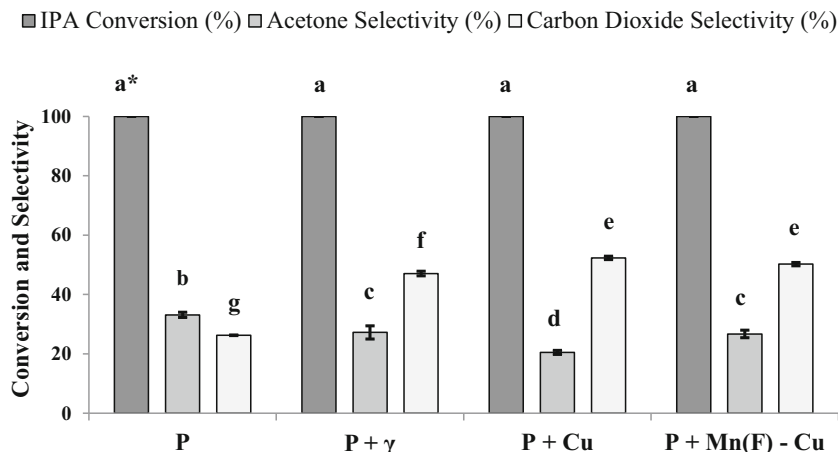
Figure 6 presents the comparison of different oxygen content in carrier gases. The oxygen content of 0% produced poor

results for the three parameters. The gas introduced was presumed to be nitrogen, and nitrogen cannot produce strong active substances such as ozone to oxidize or convert IPA (Shiau et al. 2017). The oxygen content of 20% and 100% provided favorable results with the increase in the oxygen content of the carrier gas. This result is consistent with that reported in the literature (Kim et al. 2008). The increase in the oxygen content of the carrier gas was speculated to increase ozone generation. Figure 7 reveals that the increased oxygen content of the carrier gas can led to more ozone generation. Subsequently, active sites on the catalyst decomposed ozone into more O_2^- or O_2^{2-}, which reacted with IPA and acetone or other intermediate products, causing an increase in the carbon dioxide selectivity.

Comparison of different reaction procedures under optimal operating conditions

Operating conditions were as follows: air temperature, 26 °C; dry air; carrier gas oxygen content, 100%; discharge gap, 3 mm; and oxidation time, 60 min. The most suitable catalyst

Fig. 8 Comparison between different reaction procedures under optimal operating conditions at 60 min

Mn (F)-Cu/γ-Al$_2$O$_3$ and carrier gas oxygen content 100% obtained from the experiments were comprehensively compared with different reaction procedures under optimal operating conditions. Figure 8 presents the comparison between different reaction procedures obtained under optimal operating conditions.

For 100% oxygen, P + Cu exhibited a satisfactory effect. At 60 min, IPA conversion rate was 100%, and carbon balance reached approximately 72.83%. Moreover, P + Mn (F)-Cu reached 100% with 100% oxygen, and the carbon balance reached approximately 76.94% at 60 min. Approximately 25% of the carbon balance was not calculated in the two reaction procedures, which was presumed to be contributed by the incomplete oxidation of carbon monoxide and trace acetaldehyde and formic acid found in GC-MS (Sivachandiran et al. 2015).

Conclusion

In the analysis of catalyst characteristics, SEM results proved that γ-Al$_2$O$_3$-supported metal oxides formed crystals on the surface, and S$_{BET}$ gradually decreased with the supported metal oxides, indicating that metal oxides were well supported on γ-Al$_2$O$_3$. By comparing various reaction procedures, except for P + Cu, the IPA conversion in all reaction procedures was 99.99%. However, P + Cu revealed favorable results for acetone and carbon dioxide selectivity. P + Mn (F)-Cu was the most effective in all the three parameters. In terms of the effect of oxygen content present in the carrier gas on the metal catalyst combined with the plasma system, 100% oxygen can lead to more satisfactory IPA conversion and acetone and carbon dioxide selectivity. However, the ozone concentration was the highest at the tail. In terms of comparison between different reaction procedures conducted under the best operating conditions, each reaction procedure provided 99.99% IPA conversion; however, P + Cu exhibited more favorable acetone and carbon dioxide selectivity. IPA conversion in procedures with P + Mn (F)-Cu was faster than that in other reaction procedures, and the ozone concentration in the tail was lower than that in other reaction procedures.

Compliance with ethical standards

Conflict of interest The authors declare that they have no conflict of interest.

References

Belaissaoui B, Le MY, Favre E (2016) Energy efficiency of a hybrid membrane/condensation process for VOC (Volatile Organic Compounds) recovery from air: A generic approach. Energy 95: 291–302

Debono O, Gaudion V, Redon N, Locoge N, Thevenet F (2018) Photocatalytic treatment of VOC industrial emissions: IPA removal using a sensor-instrumented reactor. Chem Eng J 353:394–409

Dhandapani B, Oyama ST (1997) Gas phase ozone decomposition catalysts. Appl Catal B Environ 11:129–166

Eliasson B, Hirth M, Kogelschatz U (1987) Ozone synthesis from oxygen in dielectric barrier discharges. J Phys D Appl Phys 20:1421–1437

Huang L, Zhu Y, Huo C, Zheng H, Feng G, Zhang C (2008) Mechanistic insight into the heterogeneous catalytic transfer hydrogenation over Cu/Al$_2$O$_3$: Direct evidence for the assistant role of support. J Mol Catal A Chem 288:109–115

Khan FI, Kr Ghoshal A (2000) Removal of volatile organic compounds from polluted air. J Loss Prev Process Ind 13(6):527–545

Kim H-H, Ogata A, Futamura S (2008) Oxygen partial pressure-dependent behavior of various catalysts for the total oxidation of VOCs using cycled system of adsorption and oxygen plasma. Appl Catal B Environ 79:356–367

Li W, Gibbs G, Oyama ST (1998) Mechanism of ozone decomposition on a manganese oxide catalyst. 1. In situ Raman spectroscopy and ab initio molecular orbital calculations. J Am Chem Soc 120:9041–9046

Li Y, Fan Z, Shi J, Liu Z, Shangguan W (2014) Post plasma-catalysis for VOCs degradation over different phase structure MnO$_2$ catalysts. Chem Eng J 241:251–258

Li S, Dang X, Yu X, Abbas G, Zhang Q, Cao L (2020) The application of dielectric barrier discharge non-thermal plasma in VOCs abatement: A review. Chem Eng J 388:124275

Malik MA, Minamitani Y, Schoenbach KH (2005) Comparison of catalytic activity of aluminum oxide and silica gel for decomposition of volatile organic compounds (VOCs) in a plasmacatalytic Reactor. IEEE Transactions on Plasma Science 33(1):50–56

Mohamed EF, Awad G, Andriantsiferana C, El-Diwany AIJE (2016) Biofiltration technology for the removal of toluene from polluted air using. Streptomyces griseus 37(10):1197–1207

Ohshima T, Kondo T, Kitajima N, Sato MJIToIA (2010) Adsorption and plasma decomposition of gaseous acetaldehyde on fibrous activated carbon 46(1):23-28.

Qin C, Huang X, Dang X, Huang J, Teng J, Kang Z (2016) Toluene removal by sequential adsorption-plasma catalytic process: effects of Ag and Mn impregnation sequence on Ag-Mn/gamma-Al$_2$O$_3$. Chemosphere 162:125–130

Rodrigo H, Tan BH, Allen NL (2005) Negative and positive impulse corona development along cylindrical insulator surfaces. IEE Proceedings - Science, Measurement and Technology 152(5):201–206

Shiau CH, Pan KL, Yu SJ, Yan SY, Chang MB (2017) Desorption of isopropyl alcohol from adsorbent with non-thermal plasma. Environ Technol 38:2314–2323

Sivachandiran L, Thevenet F, Rousseau A (2014) Regeneration of isopropyl alcohol saturated MnXOY surface: comparison of thermal, ozonolysis and non-thermal plasma treatments. Chem Eng J 246: 184–195

Sivachandiran L, Thevenet F, Rousseau A (2015) Isopropanol removal using MnXOY packed bed non-thermal plasma reactor: Comparison between continuous treatment and sequential sorption/regeneration. Chem Eng J 270:327–335

Spasova I, Nikolov P, Mehandjiev D (2007) Ozone decomposition over alumina-supported copper, manganese and copper-manganese catalysts. Ozone Sci Eng 29:41–45

Sudhakaran MSP, Trinh HQ, Karuppiah J, Hossian MM, Mok YS (2017) Plasma catalytic removal of p-xylene from air stream using γ-Al_2O_3 supported manganese catalyst. Top Catal 60:944–954

Tahir D, Ilyas S, Abdullah B, Armynah B, Kim K, Kang HJ (2018) Modification in electronic, structural, and magnetic properties based on composition of composites copper (II) oxide (CuO) and carbonaceous material. Materials Research Express 6

Tang X, Feng F, Ye L, Zhang X, Huang Y, Liu Z (2013) Removal of dilute VOCs in air by post-plasma catalysis over Ag-based composite oxide catalysts. Catal Today 211:39–43

Todorova S, Kolev H, Holgado JP, Kadinov G, Bonev C, Pereñíguez R (2010) Complete n-hexane oxidation over supported Mn–Co catalysts. Appl Catal B Environ 94:46–54

Vandenbroucke AM, Morent R, De Geyter N, Leys C (2011) Non-thermal plasmas for non-catalytic and catalytic VOC abatement. J Hazard Mater 195:30–54

Wang T, Chen S, Wang H, Liu Z, Wu Z (2017) In-plasma catalytic degradation of toluene over different MnO 2 polymorphs and study of reaction mechanism. Chin J Catal 38:793–803

Wang B, Xu X, Xu W, Wang N, Xiao H, Sun Y (2018) The mechanism of non-thermal plasma catalysis on volatile organic compounds removal. Catal Surv Jpn 22:73–94

Zakaria ZY, Linnekoski J, Amin NAS (2012) Catalyst screening for conversion of glycerol to light olefins. Chem Eng J 207-208:803–813

Zhu X, Gao X, Yu X, Zheng C, Tu X (2015) Catalyst screening for acetone removal in a single-stage plasma-catalysis system. Catal Today 256:108–114

Zhu X, Tu X, Mei D, Zheng C, Zhou J, Gao X (2016) Investigation of hybrid plasma-catalytic removal of acetone over CuO/gamma-Al_2O_3 catalysts using response surface method. Chemosphere 155:9–17